On the variation of magnetic anisotropy in Co/Pt(111) on silicon oxide

G. Winkler, A. Kobs, A. Chuvilin, D. Lott, A. Schreyer, and H. P. Oepen

Citation: Journal of Applied Physics **117**, 105306 (2015); doi: 10.1063/1.4914039
View online: http://dx.doi.org/10.1063/1.4914039
View Table of Contents: http://scitation.aip.org/content/aip/journal/jap/117/10?ver=pdfcov
Published by the AIP Publishing

On the variation of magnetic anisotropy in Co/Pt(111) on silicon oxide

G. Winkler,[1] A. Kobs,[1] A. Chuvilin,[2,3] D. Lott,[4] A. Schreyer,[4] and H. P. Oepen[1]
[1]*Institut für Nanostruktur und Festkörperphysik, Universität Hamburg, Jungiusstr. 11, D-20355 Hamburg, Germany*
[2]*CIC nanoGUNE Consolider, Av. de Tolosa 76, E-20018 Donostia–San Sebastián, Spain*
[3]*Ikerbasque, Basque Foundation for Science, 48013 Bilbao, Spain*
[4]*Helmholtz-Zentrum Geesthacht, Zentrum für Material- und Küstenforschung GmbH Max-Planck-Straße 1, D-21502 Geesthacht, Germany*

(Received 23 October 2014; accepted 21 February 2015; published online 12 March 2015)

The structural properties and magnetic anisotropy of Pt/Co/Pt trilayers grown on thermally oxidized (Si/SiO_2) and naturally oxidized silicon (Si/Si_{ox}) are presented. Although similar substrates and identical preparation conditions are used distinct differences in the structural composition are found which stem from the Pt seed layer created via ion assisted sputtering. While for thermal oxidized Si a Pt/Co/Pt trilayer is formed, for systems grown on naturally oxidized Si a complex PtSi alloy formation within the seed layer is observed as a consequence of the high ion energies of ion assisted sputtering. The composition of the PtSi alloy varies along the growth direction with a low Si content at the interface to Co and the lattice constant is similar to bulk Pt. The latter provides a much higher magnetic interface anisotropy constant compared to Pt/Co/Pt on thermal oxidized Si of about 0.9 mJ/m^2 which is comparable to the highest values found for MBE grown Co on single crystalline Pt(111). © *2015 AIP Publishing LLC*.
[http://dx.doi.org/10.1063/1.4914039]

I. INTRODUCTION

The fabrication of magnetic multilayers with high perpendicular magnetic anisotropy (PMA) has been a challenge for decades. It is found that the magnetic properties depend strongly on the quality of the films and interfaces which in turn are highly affected by the preparation conditions. Accordingly, the published values for magnetic surface and volume anisotropy constants of Co/Pt multilayers span a large range. The strongest impact has the preparation method, e.g. MBE grown films[1–3] generally exhibit higher anisotropy constants than polycrystalline films prepared by sputter deposition techniques.[2–6] Apart from the preparation method, further approaches to enhance the PMA include the reduction of substrate roughness,[7,8] reduction of intermixing at the interface,[9,10] or the choice of seed layer.[11] In this context, rather intensive substrate and seed layer preparation procedures have been applied to improve the sample quality and PMA.

In this paper, we report on Co/Pt multilayers grown simultaneously on naturally (Si/Si_{ox} (2 nm)) and thermally oxidized silicon (Si/SiO_2 (300 nm)). We used our standard preparation procedure that is reported in detail in Ref. 12. A Pt seed layer is deposited via ion beam sputtering utilizing an electron cyclotron resonance (ECR) source,[13] while the successive layers are grown via DC magnetron sputtering. The ECR seed layer has the smallest thickness ($t_{Pt,ECR} = 4$ nm) that guarantees magnetic properties independent on seed layer thickness.[12] On the ECR film, a 1 nm thick Pt layer and a Co film of varying thickness (0.8 – 9 nm, 50 nm) are deposited capped by a Pt layer (3 nm).

In the light of the previous reported results on Co/Pt, we demonstrate that very different magnetic properties are attained even for samples prepared on very similar substrates. To emphasize the latter issue, we first present the results of the magnetic characterization. The in-plane and out-of-plane magnetization curves are measured by means of longitudinal and polar magneto-optic Kerr-effect (MOKE). In Fig. 1 hard axis magnetization curves are shown for samples with an easy axis (a) out-of-plane and (b) in plane, respectively. From these curves, the magnetic anisotropy constants in second order approximation are determined[14] utilizing the saturation magnetization of bulk Co ($M_S = 1.4 \cdot 10^6$ A/m).[15,17] The insets in Figs. 1(a) and 1(b) show the corresponding easy axis loops. For the second order anisotropy constant K_2 values in the range of (70 ± 30) kJ/m^3 are found independent of substrate and Co thickness.[18,19] The values are in good accordance with published numbers for K_2 of Co/Pt systems.[5,20] The product of first order anisotropy and thickness, $t_{Co} \cdot K_{1,eff}$, is plotted in Fig. 1(c) versus Co thickness t_{Co} for sandwiches grown on both kind of substrates. Straight lines with almost identical slopes are obtained. The linear dependence indicates that a simple phenomenological model can be applied to fit the data that separates bulk ($K_{1V,eff}$) and surface/interface contributions (K_S) to the magnetic anisotropy

$$K_{1,\mathrm{eff}}(t_{\mathrm{Co}}) \cdot t_{\mathrm{Co}} = \underbrace{\left(K_{1V} - \frac{\mu_0}{2} M_S^2\right)}_{K_{1V,\mathrm{eff}}} t_{\mathrm{Co}} + 2K_S.$$

Within the model, the similar slope of the two fits means that the bulk properties of both sandwiches are very much the same, while on the other hand, the surface contributions are different. Obviously, $K_{1,eff}$ is higher for Si_{ox} than for SiO_2 for any given t_{Co}, which means that the interface anisotropy constant K_S is higher for Si_{ox} than for SiO_2 (see inset of Fig.

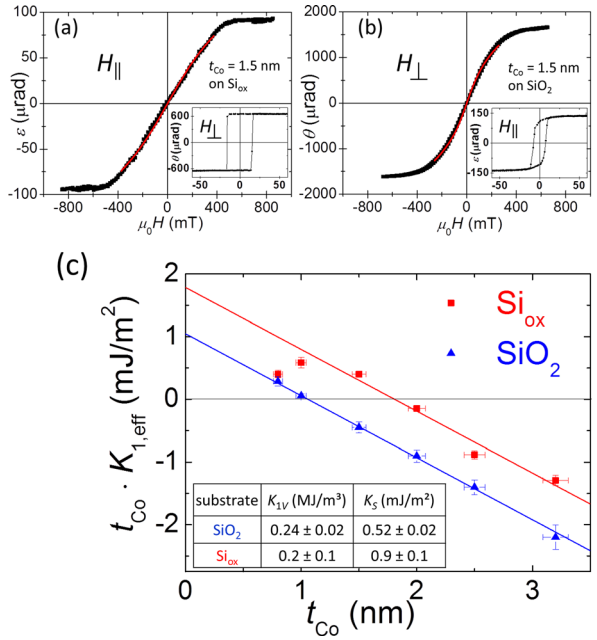

FIG. 1. MOKE investigation of Pt (5 nm)/Co (t_{Co})/Pt (3 nm) sandwiches. (a) Longitudinal Kerr ellipticity (loop with field in-plane) for the sample on naturally oxidized silicon (Si_{ox}) and (b) polar Kerr rotation (field perpendicular to film) on thermally oxidized silicon (SiO_2) with $t_{Co} = 1.5$ nm. The red solid lines are fits to the hard axis curves assuming coherent rotation of magnetization using anisotropy terms up to the second order.[14] The insets show the corresponding easy axis curves for both samples. (c) shows the effective first order anisotropy constant $K_{1,eff}$ times Co thickness t_{Co} versus t_{Co} for sandwiches grown on Si_{ox} (red) and SiO_2 (blue). The solid lines are linear fits to the data. The value for $t_{Co} = 0.8$ nm is not considered for the fit in case of Si_{ox}. The inset shows the volume anisotropy constant K_{1V} and interface anisotropy constant K_S determined from the fits utilizing $M_S = 1.4 \cdot 10^6$ A/m.

1). The values are in the range of data reported in the literature for Co/Pt(111) layered structures,[21,22] while $K_S = (0.9 \pm 0.1)$ mJ/m^2 for Si_{ox} fits within the span of values found for MBE grown Co/Pt(111) systems (0.8–1.3 mJ/m^2).[1–3,23,24] Besides the higher surface anisotropy, another difference is found at low Co thicknesses. While for the Pt/Co/Pt grown on SiO_2, the linear behavior is observed in the whole thickness range a drop of the anisotropy is found in the second system at low thicknesses. The deviation from the linear behavior of $K_{1,eff}(t_{Co}) \cdot t_{Co}$ below $t_{Co} \approx 1$ nm is frequently reported for Co/Pt. Its origin is attributed to variations in strain,[25] a decrease in the Curie temperature,[2,23] or to the low thickness of the layer that falls below the interface roughness and the depth of interdiffusion.[2,10,21]

To make the point: Although our preparation conditions for the growth on both substrates are absolutely identical strongly differing magnetic properties are found. Even though the substrates are apparently equivalent, they have to have an impact on the magnetic properties. To clarify the latter puzzle, the structure of the multilayers is investigated.

II. STRUCTURAL PROPERTIES

The structural properties are investigated by X-ray diffraction (XRD) and reflectometry (XRR) utilizing the Cu-Kα line (1.5406 Å). Structure and composition of the stacks are studied by high resolution transmission electron microscopy (HRTEM) and high resolution element mapping utilizing energy dispersive X-ray spectroscopy (EDX) in the scanning TEM mode of the electron microscope.[26] Cross sections of the samples are made by focused ion beam (FIB) technique following a standard protocol for TEM lamellae preparation. Prior to FIB cutting 10 nm of carbon and a thick Pt layer is deposited to protect the multilayer during FIB cutting. The preparation and all experiments are performed at room temperature. The thicknesses of the oxides on the silicon substrates are determined via ellipsometry yielding (300 ± 3) nm for SiO_2 and (2.0 ± 0.5) nm for Si_{ox}.

A. HRTEM investigation

Cross-sectional HRTEM investigations in combination with energy-dispersive X-ray spectroscopy (EDX) are made. Cross-sections of sandwiches grown on the two different substrates are shown in Figs. 2(a)–2(f) for different thicknesses of the Co layer. The lamellae (thickness = 25 nm) have twice the extent of the lateral grain size of (11 ± 2) nm, which is determined via scanning electron microscopy. Hence, the observed lattice patterns represent a superposition of the structure of a few grains.

The Pt/Co/Pt sandwich structure grown on top of a SiO_2 substrate is shown in Figs. 2(a) and 2(c). The surface of the substrate exhibits a slight corrugation that is cloned into the following interfaces, i.e., Pt/Co, Co/Pt, and Pt/C. Besides, these mesoscopic corrugations caused by the substrate, the interfaces appear sharp. While for films on SiO_2 three layers are found (Pt/Co/Pt), as expected, the multilayer on Si_{ox} exhibits five layers (see Figs. 2(b), 2(d), and 2(f)). The EDX analysis (Fig. 2(e)) reveals that two PtSi layers are formed that are separated by a third layer. Presumably, the intercalated layer is a mixture of the natural silicon oxide and the deposited Pt. The oxygen content is not plotted in Fig. 2(e) as its intensity is too small to be separated from the background signal. Nonetheless, the drop in the Pt and Si signal indicates the presence of a third species in this region. The upper PtSi layer reveals a Si gradient in the stacking direction. The Si/Pt ratio at the oxide/PtSi interface, which is the same as in the lower PtSi layer, decreases to nearly zero at the PtSi/Co interface. Hence, the Co grows on a surface that consists almost entirely of Pt. The formation of a PtSi alloy has been previously reported when Si/Pt samples are heated during or after deposition of Pt on Si.[27–30] Intermixing of Si and sputter deposited Pt, however, has not been reported so far for Co/Pt films prepared by magnetron sputtering on Si_{ox} at room temperature.[23,31]

The EDX analysis (Fig. 2(e)) reveals that a considerable amount of Pt penetrates into the single-crystalline Si substrate (penetration depth of about 5 nm). This finding is confirmed by the contrast in the micrograph of Fig. 2(g) which is obtained utilizing HAADF STEM (High Angle Annular Dark Field Scanning Transmission Electron Microscopy). As dark field images give a sharp composition contrast,[32] the decreasing intensity with increasing distance from the interface illustrates the decreasing Pt content in the Si. Both the EDX profile (yellow) and the dark field image reveal the same structure which emphasizes the penetration of Pt into the Si.

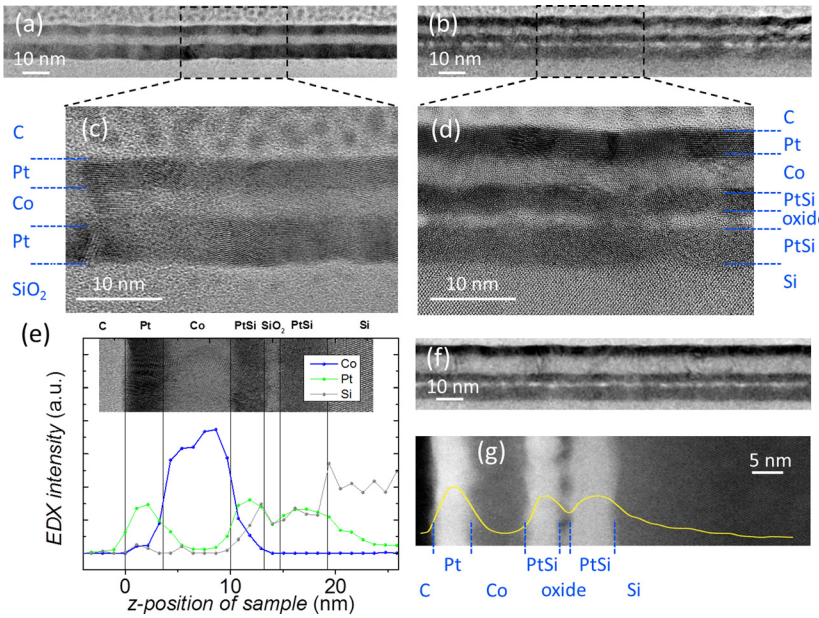

FIG. 2. HRTEM investigation of Pt (5 nm)/Co (t_{Co})/Pt (3 nm) sandwiches. Micrographs (a) and (b) display the cross-sections of films with $t_{Co} = 5$ nm grown on SiO_2 and Si_{ox}, respectively. The images (c) and (d) show zooms into the structure displayed in (a) and (b), respectively. While on SiO_2 the stack is a trilayer, on Si_{ox} two PtSi layers appear which are separated by a PtSi-oxide layer. Panel (e) gives an EDX cross-section of the film with $t_{Co} = 9$ nm grown on Si_{ox}. (f) shows the corresponding micrograph while panel (g) displays a HAADF STEM image with the Pt concentration profile from EDX (yellow).

The HRTEM measurements further demonstrate that the lower PtSi layer does not show any lattice fringes (see Fig. 2(d)), which indicates that it is amorphous. On the other hand, the upper PtSi layer clearly contains crystal fringes, which proceed through the Co up to the Pt cap layer (see Fig. 2(d)). This indicates that successive Co and Pt layers grow in a crystalline phase on the upper most crystalline part of the seed layer. On SiO_2 the crystallinity is found in all three layers (see Fig. 2(c)).

B. X-ray investigation

The HRTEM measurements give a good insight into the local structure. To obtain the averaged structural properties over a macroscopic lateral scale X-ray reflectometry (XRR) and diffraction (XRD) are carried out. In Fig. 3(a), the specularly reflected X-ray intensity is plotted versus the scattering vector $Q_z = 4\pi/\lambda \sin\theta$, where θ is the reflection angle. Shown are the results obtained from sandwiches deposited on both SiO_2 and Si_{ox} substrates ($t_{Co} = 3.2$ nm). The curves for SiO_2 (blue) and Si_{ox} (red) are fitted by applying Parratt's recursive formalism[33–35] taking the results of the TEM analysis into account, i.e., assuming a Pt/Co/Pt and a PtSi/PtSi-oxide/PtSi/Co/Pt stack for the sandwiches on SiO_2 and Si_{ox} substrates, respectively. For the fitting, minor variations of the layer thicknesses obtained by TEM as well as small changes of the scattering length densities (assuming bulk values[36,37]) are tolerated. The fits (black solid lines) reproduce the data for both substrates very well (Fig. 3(a)). The fitting procedure provides values for the width of the roughness and zone of interdiffusion σ at the interfaces of $\sigma = (3 \pm 1)$ monolayers. Off-specular scans allow for the separation of roughness and intermixing as the latter does not give rise to off-specular scattering. The results indicate that the films are very smooth with a roughness of about one monolayer, so that σ is dominated by the CoPt interdiffusion zone (not shown). The XRR results prove that PtSi layers are present also on a large scale for the sandwiches grown on Si_{ox}. Hence, the HRTEM investigations can be taken as characteristic for the sample. On the other hand, the X-ray reflectivity curve can only be fitted reasonably well for the multilayers on SiO_2 when assuming a pure Pt/Co/Pt trilayer. The latter confirms that PtSi formation is prevented by the thick oxide layer.

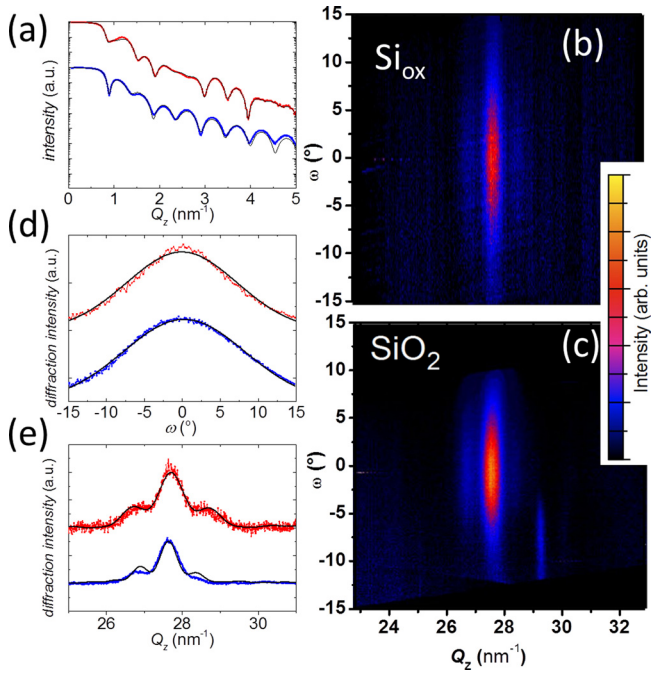

FIG. 3. X-ray investigation of Pt (5 nm)/Co (3.2 nm)/Pt (3 nm). Plot (a) gives the results of X-ray reflectometry measurements on Si_{ox} (red line) and SiO_2 (blue line). The black solid lines are fits to the curves utilizing Parratt's recursive formalism. Images (b) and (c) are diffraction maps $I(Q_z,\omega)$ for SiO_2 (b) and Si_{ox} (c), respectively, showing the Pt(111) peak. The intensity peaks that are not centered around $\omega = 0°$ are artifacts caused by the experimental set-up. (d) displays the integrated intensity $I(\omega) = \sum_{Q_z} I(\omega, Q_z)$ in the range $Q_z = 2.7 - 2.8$ Å^{-1} for Si_{ox} (red) and SiO_2 (blue). The black lines are Gaussian fits. Plot (e) displays XRD scans $I(Q_z,\omega = 0)$ for Si_{ox} (red) SiO_2 (blue). The black lines represent the results of the fitting using the kinematic approximation.

The crystallinity of the samples is analyzed by high angle X-ray diffraction (XRD). Rocking scans are performed in which the sample is rotated (angle ω) about the axis perpendicular to the scattering plane (fixed 2θ angle). $\omega = 0°$ represents the classical 2θ-geometry with θ measured with respect to the normal of the macroscopic surface. Intensity maps $I(\omega,Q_z)$ are shown in Figs. 3(b) and 3(c) for equal Co thickness (3.2 nm) grown on the two substrates. In the plot, the range of scattering vectors of $2.283\,\text{Å}^{-1} < Q_z < 3.285\,\text{Å}^{-1}$ is shown, where fcc Pt(111), fcc Co(111), and hcp Co(0001) bulk diffraction peaks must show up. For both substrates intensity peaks are observed in the vicinity of the fcc Pt(111) bulk position ($Q_z = 2.776\,\text{Å}^{-1}$), while no traces of diffraction intensities due to Co are found. The latter comes from the fact that the Co thickness is small and Co has a much smaller scattering cross-section than Pt.[38] The maximum of the Pt(111) peaks is always located at $\omega \approx 0°$ which becomes evident with the plot of the integrated intensity $I(\omega) = \sum_{Q_z} I(\omega, Q_z)$ created from the maps (Fig. 3(d)). The plots demonstrate a preferential [111] orientation of the Pt crystallites. Further evidence for the pronounced Pt(111) texture is the absence of the Pt(200) peak at $Q_z = 3.205\,\text{Å}^{-1}$ (in Fig. 3(b)/3(c)) which should appear for a random orientation of crystallites.[38] The distribution of the orientation of the grains is well fitted by a Gaussian (Fig. 3(d)). A quantitative measure of the degree of texture is the full width at half maximum b_ω. On SiO_2 the Pt (111) peak is slightly wider (FWHM: $b_\omega = (23 \pm 2)°$) than on Si_{ox} ($b_\omega = (15 \pm 3)°$) meaning that on Si_{ox} the (111)-texture is more pronounced than on SiO_2.

The cross-section of the diffraction maps, $I(Q_z)$ at $\omega = 0°$, is plotted in Fig. 3(e). Two small satellites on both sides of the Pt(111) peak are caused by the variation of the material in the perpendicular direction, i.e., a result of the layered structure.[39] The profile $I(Q_z)$ is modeled within the kinematic approximation.[40,41] In accordance with the HRTEM investigation, the best fit can be obtained by assuming a Pt/Co/Pt and a (amorphous) PtSi/(amorphous) PtSi-oxide/PtSi/Co/Pt stack for the sandwiches on SiO_2 and Si_{ox} substrate, respectively. Only the latter three crystalline layers (PtSi/Co/Pt) contribute to the scattering in the range of $Q_z = 2.776\,\text{Å}^{-1}$. The fit yields the total thickness of the crystalline constituents from which the thickness of the crystalline PtSi can be estimated. Taking the nominal thicknesses for the Co film and the Pt cap layer, we obtain for the crystalline PtSi layer $t_{\text{seed,Siox}} = (3 \pm 1)$ nm. The value is significantly smaller than the thickness of the crystalline seed layer on SiO_2 ($t_{\text{seed,SiO}_2} = (5.0 \pm 0.1)$ nm) and fits very well the thickness of that layer obtained from the HRTEM image.

Another striking difference between the plots in Fig. 3(e) is the position of the main peak which indicates that the two seed layers have different lattice parameter. On SiO_2, the peak is at $Q_z = (2.757 \pm 0.003)\,\text{Å}^{-1}$ while for Pt grown on Si_{ox} it is at $Q_z = (2.769 \pm 0.003)\,\text{Å}^{-1}$, which gives a lattice spacing of $d_{\text{Pt(111),SiO}_2} = (0.2278 \pm 0.0003)$ nm and $d_{\text{Pt(111),Siox}} = (0.2269 \pm 0.0003)$ nm, respectively. The value for Pt on Si_{ox} is very close to the value of bulk Pt $d_{\text{Pt,bulk}} = 0.2263$ nm, while for SiO_2, the interplanar spacing of the Pt layers is expanded by 0.7% compared to bulk Pt. Hence, it can be concluded that Co deposition on Pt/Si_{ox} is comparable to Co grown on Pt(111). The surface anisotropy that is attained here is indeed very close to the maximum values published for Co/Pt(111).[1,3]

So far PtSi alloying has not been reported for magnetron sputtered Co/Pt films grown on Si at room temperature. To cross-check our results magnetron sputtered Pt (5 nm)/Co (2 nm)/Pt (3 nm) trilayers are prepared and investigated via XRD and XRR. The spectra for layers produced on Si_{ox} and SiO_2 do not show any significant difference which indicates that PtSi and the intercalated oxide does not exist (not shown). The latter results document that the high energy of the ions in the ECR sputtering causes the PtSi formation. Note that for thinner ECR seed layer thicknesses ($t_{\text{Pt,ECR seed}} < 4$ nm), we observe that the magnetic anisotropy significantly decreases, which might be a consequence of CoSi alloy formation as the enthalpy of formation for PtSi and CoSi are comparable.[42] The microscopic mechanism that drives the Pt into the Si lattice in the ECR sputtering is not clear and outside the focus of the study. Two processes can be imagined: (a) the Pt particles with energy of about 20 eV (Ref. 43) directly penetrate and/or (b) high energy Ar^+-ions ($\leq$1.2 keV) reaching the substrate enforce the intermixing and the creation of pinholes in the thin natural oxide. Through the pinholes the Si can diffuse outward and the Pt vice versa inward.

To answer the question whether the Co grows in hcp or fcc structure, XRD scans are performed by varying the angle between film normal and plane of incidence (not shown). To overcome the small signals of the Co peaks, the Co thickness is increased to $t_{\text{Co}} = 50$ nm. The scattering intensities show the characteristics of the fcc phase and no hcp features. This result is in accordance with the value for the volume contribution to magnetic anisotropy obtained from the plot in Fig. 1, which are $K_V = (0.24 \pm 0.02)\,\text{MJ/m}^3$ for SiO_2 and $(0.2 \pm 0.1)\,\text{MJ/m}^3$ for Si_{ox}. The found anisotropy constants are smaller than the literature values for hcp Co ($K_{V,\text{hcp}} \approx 0.5\,\text{MJ/m}^3$ (Ref. 16)) but larger than the literature values of fcc Co ($K_{V,\text{fcc}} \approx 0.02\,\text{MJ/m}^3$ (Ref. 44)). As the seed layer can only cause a tensile in-plane strain in the Co layer, which strengthens the out of plane anisotropy,[45,46] this is in accordance with the fact that the Co is in its fcc phase.

III. DISCUSSION OF THE DIFFERENCE IN SURFACE ANISOTROPY CONSTANT

According to the above results, the splitting of the stack into homogeneous bulk parts separated by sharp interfaces seems to be justified. Utilizing this model, we discuss possible structural origins (texture, roughness, alloying, and strain at the interface) for the strong difference in K_S of 0.4 mJ/m^2 between both substrates (Fig. 1).

For crystalline Co/Pt layered structures, the dependence of K_S on interface orientation has been reported.[23,49,50] A change from (111) to (110) orientation of the CoPt multilayers causes a drop of K_S by 0.55 mJ/m^2.[49] A theoretical estimation has given a decrease of 0.15 mJ/m^2.[50] The mean tilting of the crystallites $\bar{\alpha}$ can be estimated by $\bar{\alpha} < \sigma = b_\omega/(2\sqrt{2\ln 2})$, yielding $\bar{\alpha}_{Siox} < 6°$ and $\bar{\alpha}_{SiO2} < 10°$. The difference in texture is even smaller (about 4°). Hence, it appears unrealistic (in the light of the above mentioned

results) to ascribe the change of 0.4 mJ/m^2 to that small angle deviation.

The interfacial roughness can cause a reduction of K_S as proposed by Bruno.[7] The relative change is given as a function of lateral coherence length L and modulation amplitude σ, i.e., $\Delta K_S/K_S = -2\sigma/L$. Taking the geometries from the HRTEM picture (Fig. 2), $L_{SiO_2} = (14 \pm 2)$ nm and $\sigma_{corr,SiO_2} = (1.0 \pm 0.3)$ nm, we obtain a relative reduction of $\Delta K_S/K_{S,Siox} = (14 \pm 11)\%$, which corresponds to $\Delta K_S = 0.13$ mJ/m^2. As the modulation for Si_{ox} is similar the difference in K_S will be even smaller than the above value and thus far below the observed ΔK_S of 0.4 mJ/m^2.

The significant difference of 0.7% in the lattice constant of the Pt seed might influence the creation of the CoPt alloy at the interface. Such alloys can cause contributions to an effective interface anisotropy $K_{S,CoPt,eff}$. Then, the difference in K_S is the product of interface thickness times the difference of the bulk anisotropy values of the two presumable alloys. For $\Delta K_S = 0.4$ mJ/m^2, we expect a difference in the bulk values of $\Delta K_{1V,CoPt} \approx 0.6$ MJ/m^3 using the thickness of the interdiffusion zone σ determined via XRR.

The observation of $Co_{1-x}Pt_x$ alloy formation at the interfaces is in line with previous studies dealing with sputtered Co/Pt films.[2,51] The published values of the volume anisotropies of homogeneous, disordered $Co_{1-x}Pt_x$ alloys, however, are considerably lower than $\Delta K_{1V,CoPt}$, namely, $K_{1V} \approx 0.3$ MJ/m^3 (Refs. 52–54) is found independent of the stoichiometry.[53] If, however, the $L1_1$ configuration of CoPt(111) appears at the Pt/Co interface on the Si_{ox} substrate the strong difference in $\Delta K_{1V,CoPt}$ would be understandable as the $L1_1$ phase is known to have a strong anisotropy due to a tetragonal distortion of the lattice.[55–58]

Due to the strong lattice mismatch between Co and Pt, a large strain can be expected in crystalline growth[10,25] (coherent thickness regime). As a large amount of energy is stored in the strained lattice the system tends to relax via creation of misfit dislocations (incoherent regime).[59] Even in case of lattice mismatch in the range of 10% a very thin coherent regime was found via sophisticated techniques of stress measurements.[48,60,61] In case of small lattice mismatch, the coherent-incoherent transition leads to a kink in the $K_{1,eff}(t_{Co}) \cdot t_{Co}$ plots which shows up far above the monolayer range (e.g. at $t_{Ni} = 1.3$–1.5 nm for Ni on Cu).[40,62]

The most obvious difference between the two plots in Fig. 1 is the deviation of $K_{1,eff}(t_{Co}) \cdot t_{Co}$ from the linear behavior for $t_{Co} \leq 1.1$ nm for sandwiches grown on Si_{ox}, while the deviation is not found on SiO_2. With the above considerations, it seems reasonable to assume for PtSi/PtSi-oxide/PtSi/Co/Pt a broad coherent regime (up to 1.1 nm) while for Pt/Co/Pt on SiO_2 the transition is well below 1 nm. Due to the larger thickness of a strained interface region, the PtSi/oxide/PtSi/Co/Pt should exhibit a stronger contribution to K_S. Importantly, a tensile strain in the (111) plane leads to a magnetoelastic contribution favoring a [111] orientation of magnetization as observed experimentally, no matter whether it is strain in Co or in $Co_{1-x}Pt_x$ alloy as the relevant parameters, i.e., magnetostriction and elastic constants, are similar.[47,63] Quantitatively, the difference in K_S can be explained by a difference in strain in the order of 5% using the constants of Ref. 45.

In the above considerations, both interfaces (Pt/Co and Co/Pt) are treated as equal, i.e., giving the same contribution to the magnetic anisotropy. Assuming that the interfaces of Co and cap layer are the same for both substrates exhibiting the K_S value of Pt/Co/Pt on SiO_2 a large interface contribution of $\Delta K_S = 0.8$ mJ/m^2 has to be appointed to the interface between Co and Pt seed layer created on Si_{ox}.

IV. CONCLUSION

In conclusion, we find that the different thickness of oxides on silicon has a strong impact on the layer composition when Pt seed layers are created via ion assisted sputtering. While the thick oxide blocks the penetration of Pt into the Si substrate and the subsequent building of silicide, the thin oxide is intercalated between two silicide layers from which the upper one exhibits crystallinity. The upper PtSi is important as it exhibits a gradient in the Si content. The decrease of Si content towards the interface to Co allows for a better adaptation of the lattice. The topmost seed layer exhibits almost the lattice constant of bulk Pt, while for a thick oxide (SiO_2), the seed layer is more strained. It is put forward that the latter difference of the Pt template is responsible for variations in the subsequent Co growth and for the observed strong difference in the interface anisotropy. The investigation demonstrates that minor, apparently dispensable, differences of the substrate have strong effects on the magnetic anisotropy. It turns out that the latter is an extremely sensitive probe for the underlying sample structure.

ACKNOWLEDGMENTS

Cooperation with Felix Balhorn (ferromagnetic resonance) and Martin Waleczek (ellipsometry), as well as funding by DFG via Sonderforschungsbereich SFB 668 and project OE 251/7-1 "Investigation of the influence of interfaces on the magnetotransport in ultrathin films" is gratefully acknowledged. H.P.O. is thankful for excellent hospitality at CIC nanoGUNE during his research stay. He gratefully acknowledges financial support from the Basque Foundation of Science via an Ikerbasque visiting fellowship. A.C. acknowledges financial support from FEI Company (The Netherlands) within the framework of a collaborative project.

[1]N. W. E. McGee, M. T. Johnson, J. J. de Vries, and J. A. de Stegge, J. Appl. Phys. **73**, 3418 (1993).
[2]D. Weller, R. F. C. Farrow, R. F. Marks, G. R. Harp, H. Notarys, and G. Gorman, Mater. Res. Soc. Symp. Proc. **313**, 791 (1993).
[3]T. Kingetsu, J. Appl. Phys. **76**, 4267 (1994).
[4]J. H. Kim and S. C. Shin, J. Appl. Phys. **80**, 3121 (1996).
[5]M. Kisielewski, A. Maziewski, M. Tekielak, J. Ferré, S. Lemerle, V. Mathet, and C. Chappert, J. Magn. Magn. Mater. **260**, 231 (2003).
[6]J. C. Lee, C. H. Hsieh, C. C. Chang, L. W. Huang, L. K. Lin, and S. F. Lee, J. Appl. Phys. **113**, 17C714 (2013).
[7]P. Bruno, J. Phys. F **18**, 1291 (1988).
[8]M. Li, Y. P. Zhao, G. C. Wang, and H. G. Min, J. Appl. Phys. **83**, 6287 (1998).
[9]P. F. Carcia, J. Appl. Phys. **63**, 5066 (1988).
[10]S. Hashimoto, Y. Ochiai, and K. Aso, J. Appl. Phys. **66**, 4909 (1989).

[11]S. Tsunashima, M. Hasegawa, K. Nakamura, and S. Uchiyama, J. Magn. Magn. Mater. **93**, 465 (1991).
[12]H. Stillrich, C. Menk, R. Frömter, and H. P. Oepen, J. Magn. Magn. Mater. **322**, 1353 (2010).
[13]M. Wellhöfer, M. Weißenborn, R. Anton, S. Pütter, and H. P. Oepen, J. Magn. Magn. Mater. **292**, 345 (2005).
[14]The free energy density in second order approximation is given by: $E/V = K_{1,eff}\sin^2\Theta + K_2\sin^4\Theta - \mu_0 H M_S\cos\Phi$, where Θ is the angle of **M** to the outstanding axis (film normal) and Φ is the angle between **M** and **H**. If the film normal is the easy (hard) axis of magnetization a field has to be applied in any in-plane direction (along the film normal), thus $\Phi+\Theta=90°$ $(\Phi=\Theta)$. Then the equilibrium zero-torque condition $\partial(E/V)/\partial\Theta = 0$ yields: $\frac{2K_{1,eff}}{M_S}m_{||} + \frac{4K_2}{M_S}m_{||}^3 = \mu_0 H(m_{||})$ and $-\left(\frac{2K_{1,eff}}{M_S}+\frac{4K_2}{M_S}\right)m_\perp + \frac{4K_2}{M_S}m_\perp^3 = \mu_0 H(m_\perp)$, respectively.
[15]The saturation magnetization of films with $t_{Co} = 7$ nm is determined by ferromagnetic resonance. As a result for both substrates the M_S values resemble the hcp/fcc bulk value at room temperature within the resolution of the experiment.[16,17]
[16]M. B. Stearns, *Landolt-Börnstein—Group III Condensed Matter, Numerical Data and Functional Relationships in Science and Technology* (Springer-Verlag, 1986), Vol. 19a.
[17]T. Suzuki, D. Weller, C. A. Chang, R. Savoy, T. Huang, B. A. Gurney, and V. Speriosu, Appl. Phys. Lett. **64**, 2736 (1994).
[18]H. Stillrich, C. Menk, R. Fromter, and H. P. Oepen, J. Appl. Phys. **105**, 07C308 (2009).
[19]D. Stickler, R. Frömter, H. Stillrich, C. Menk, H. P. Oepen, C. Gutt, S. Streit-Nierobisch, L. M. Stadler, G. Grübel, C. Tieg, and F. Yakhou-Harris, Phys. Rev. B **84**, 104412 (2011).
[20]J. W. Lee, J. Kim, S. K. Kim, J. R. Jeong, and S. C. Shin, Phys. Rev. B **65**, 144437 (2002).
[21]W. B. Zeper, F. J. A. M. Greidanus, P. F. Carcia, and C. R. Fincher, J. Appl. Phys. **65**, 4971 (1989).
[22]F. J. A. den Broeder, W. Hoving, and P. J. H. Bloemen, J. Magn. Magn. Mater. **93**, 562 (1991).
[23]C. J. Lin, G. L. Gorman, C. H. Lee, R. F. C. Farrow, E. E. Marinero, H. V. Do, H. Notarys, and C. J. Chien, J. Magn. Magn. Mater. **93**, 194 (1991).
[24]J. Kisielewski, A. Kirilyuk, A. Stupakiewicz, A. Maziewski, A. Kimel, T. Rasing, L. T. Baczewski, and A. Wawro, Phys. Rev. B **85**, 184429 (2012).
[25]C. L. Canedy, X. W. Li, and G. Xiao, Phys. Rev. B **62**, 508 (2000).
[26]Manufacturer: FEI, Netherlands, type: TitanG2 60–300 electron microscope.
[27]H. B. Ghozlene, P. Beaufrère, and A. Authier, J. Appl. Phys. **49**, 3998 (1978).
[28]E. Conforto and P. E. Schmid, Philos. Mag. A **81**, 61 (2001).
[29]A. Hiraki, M. A. Nicolet, and J. W. Mayer, Appl. Phys. Lett. **18**, 178 (1971).
[30]J. Shi, D. Kojima, and M. Hashimoto, J. Appl. Phys. **88**, 1679 (2000).
[31]M. J. Bonder, N. D. Telling, P. J. Grundy, C. A. Faunce, T. Shen, and V. M. Vishnyakov, J. Appl. Phys. **93**, 7226 (2003).
[32]P. D. Nellist, "Scanning transmission electron microscopy," in *Science of Microscopy* (Springer, 2007).
[33]L. G. Parratt, Phys. Rev. **95**, 359 (1954).
[34]C. Braun, Parratt32 or the reflectivity tool (1997–1999).
[35]A. Nelson, J. Appl. Crystallogr. **39**, 273 (2006).
[36]Scattering lengths from Ref. 37, calculated with $\lambda = 0.15406$ nm to $\rho_{Co} = 6.308\cdot10^{-3}$ nm^{-2}, $i\rho_{Co} = 9.129\cdot10^{-4}$ nm^{-2}, $\rho_{Pt} = 1.374\cdot10^{-2}$ nm^{-2}, $i\rho_{Pt} = 1.350\cdot10^{-3}$ nm^{-2}, $\rho_{si} = 2.104\cdot10^{-3}$ nm^{-2}, $i\rho_{Si} = 4.795\cdot10^{-5}$ nm^{-2} and $\rho_{SiO_2=PtSi\text{-}oxide} = 1.982\cdot10^{-3}$ nm^{-2}, $i\rho_{SiO_2=PtSi\text{-}oxide} = 2.577\cdot10^{-5}$ nm^{-2}, $\rho_{PtSi} = 8.257\cdot10^{-3}$ nm-2, $i\rho_{PtSi} = 7.103\cdot10^{-4}$ nm^{-2}.
[37]B. L. Henke, E. M. Gullikson, and J. C. Davis, Atom. Data Nucl. Data Tables **54**(2), 181 (1993).
[38]J. A. Ibers and W. C. Hamilton, *International Tables for X-Ray Crystallography, Vol. IV Revised and Supplementary Tables to Vol. II and III* (Kluwer Academic Publishers, 1989).
[39]A. Segmüller and A. E. Blakeslee, J. Appl. Crystallogr. **6**, 19 (1973).
[40]J. A. C. Bland and B. Heinrich, *Ultrathin Magnetic Structures I, An Introduction to the Electronic, Magnetic and Structural Properties* (Springer-Verlag, 1994).
[41]The intensity of the specular scattered X-rays from a layered structure is given by $I(Q_z) = |\langle A(Q_z)|A(Q_z)^*\rangle|^2$ with the amplitude $A(Q_Z) = \sum_{j=1}^{M} f_j^{layer} e^{iQ_z r_j}$. The sum is over each of the M monolayer in the layered structure, f_j^{layer} is the layer scattering factor ($f_{layer,Pt} = 9.72$ and $f_{layer,Co} = 3.61$, f_j^{layer} corresponds to the product of atomic scattering factor ($f_{Pt} = 64.7$ and $f_{Co} = 19.5$ (Ref. 38)) and atomic density $4/(\sqrt{3}a_{fcc}^2)$ (Co: 18.5 atoms/nm^2, Pt: 15.0 atoms/nm^2)) and r_j is the position of the jth monolayer. The layer structure derived from the HRTEM measurements is used considering interface regions between the layers determined by XRR. The only fitting parameters are the interlayer distances $d_i = r_i - r_j$ for which clear boundary conditions are applied (starting values: $d_{Co,bulk} = 0.2035$ nm and $d_{Pt,bulk} = 0.2263$ nm). In case that the coherence length in growth direction is smaller than the thickness of the metallic Pt and Co layers a fraction of the intensity is given by $I(Q) = |\langle A_{Pt,seed}|A_{Pt,seed}^*\rangle|^2 + |\langle A_{Co}|A_{Co}^*\rangle|^2 + |\langle A_{Pt,cap}|A_{Pt,cap}^*\rangle|^2 + \Sigma|\langle A_{interface}|A_{interface}^*\rangle|^2$.
[42]S. V. Meschel and O. J. Kleppa, J. Alloys Compds. **267**, 128 (1998); **280**, 231 (1998).
[43]Calculated by using TRIM: J. Ziegler, J. Biersack, and U. Littmark, *The Stopping and Range of Ions in Solids* (New York, Pergamon, 1985), SRIM code:http://www.srim.org.
[44]$K_{V,fcc}$ corresponds to the energy density difference between magnetization along [111] direction (easy axis) and [100] direction (hard axis) calculated from $K_{1,cub} = -62$ kJ/m^3 and $K_{2,cub} = 0$ kJ/m^3 (Ref. 17) according to $\Delta E_{111} = 1/3 * K_{1,cub} + 1/27 * K_{2,cub}$.
[45]The magnetoelastic anisotropy contribution is given by $K_{me,fcc} = B_2(\varepsilon_0 - \varepsilon_3)$,[46] where $B_{2,Co\ fcc} = 7.7$ MJ/m^3 (Refs. 47 and 48) is the magneto-elastic constant. The out-of-plane strain $\varepsilon_3 = -0.57$ ε_0 is determined under the assumption of vanishing stress along the out-of-plane direction using $\varepsilon_3 = -2\,\varepsilon_0(c_{11} + 2c_{12} - 2c_{44})/(c_{11,} + 2c_{12} + 4c_{44})$ and $c_{11} = 242$ GPa, $c_{12} = 160$ GPa, $c_{44} = 128$ GPa.[48] c_{ij} are the elastic constant of fcc Co and ε_0 is the (isotropic) in-plane strain.
[46]D. Sander, J. Phys.-Condens. Matter **16**, R603 (2004).
[47]H. Takahashi, S. Tsunashima, S. Iwata, and S. Uchiyama, J. Magn. Magn. Mater. **126**, 282 (1993).
[48]D. Sander, Rep. Prog. Phys. **62**, 809 (1999).
[49]R. F. C. Farrow, "Chemical ordering and magnetic anisotropy in MBE grown Co/Pt multilayers," in *Magnetism and Structure in Systems of Reduced Dimensions* (Plenum Press, 1993).
[50]J. M. MacLaren and R. H. Victora, IEEE Trans. Magn. **29**, 3034 (1993).
[51]G. A. Bertero, R. Sinclair, C. H. Park, and Z. X. Shen, J. Appl. Phys. **77**, 3953 (1995).
[52]C. J. Lin and G. L. Gorman, Appl. Phys. Lett. **61**, 1600 (1992).
[53]D. Weller, H. Brändle, and C. Chappert, J. Magn. Magn. Mater. **121**, 461 (1993).
[54]S. E. Park, P. Y. Jung, and K. B. Kim, J. Appl. Phys. **77**, 2641 (1995).
[55]S. Iwata, S. Yamashita, and S. Tsunashima, IEEE Trans. Magn. **33**, 3670 (1997).
[56]F. T. Yuan, A. C. Sun, and J. H. Hsu, Scr. Mater. **62**, 762 (2010).
[57]A. Sakuma, J. Phys. Soc. Jpn. **63**, 3053 (1994).
[58]P. Ravindran, A. Kjekshus, H. Fjellvåg, P. James, L. Nordström, B. Johansson, and O. Eriksson, Phys. Rev. B **63**, 144409 (2001).
[59]J. H. van der Merwe, J. Appl. Phys. **34**, 123 (1963).
[60]A. Enders, D. Sander, and J. Kirschner, J. Appl. Phys. **85**, 5279 (1999).
[61]E. Lundgren, B. Stanka, M. Schmid, and P. Varga, Phys. Rev. B **62**, 2843 (2000).
[62]R. Jungblut, M. T. Johnson, J. aan de Stegge, A. Reinders, and F. J. A. denBroeder, J. Appl. Phys. **75**, 6424 (1994).
[63]A. G. Every and A. K. Mccurdy, *Landolt-Börnstein—Group III Condensed Matter, Second and Higher Order Elastic Constants* (Springer-Verlag, 1992), Vol. 29a.